

sible to explain the attenuation solely by decreases in the magnetic field. We also considered possible instrumental explanations for the attenuation pattern, but they failed to account for the 100-Hz observations (4).

It now appears likely that the complete explanation for the observed 100-Hz amplitude variation also involves energy transfer between the whistler mode waves and ionospheric electrons, as Landau damping and resonant cyclotron damping processes become effective (5). Landau damping is usually significant whenever the wave phase speed becomes comparable to the thermal electron speed; however, a suprathermal electron population can also produce strong damping. On orbit 4 the 100-Hz waves started to disappear when  $B$  was near  $30 \gamma$ , with the electron density  $N$  rising above  $10^3 \text{ cm}^{-3}$ . For these conditions the phase speed of a 100-Hz whistler wave is typically  $3 \times 10^5 \text{ m/sec}$ , which is comparable to the electron thermal speed when the temperature is a few thousand degrees.

When the ionopause is at low altitudes during storms, the higher density leads to small whistler wavelengths; hence absorption, refraction, or reflection can occur on much smaller distance scales. The lowest panel in Fig. 2 shows an amplitude increase of two orders of magnitude as the spacecraft altitude increased by 800 to 1600 m during a 1- to 2-second interval, when the electron density dropped significantly (3). Since  $N \approx 2 \times 10^4 \text{ cm}^{-3}$ ,  $B \approx 20$  to  $40 \gamma$ , and  $f = 100 \text{ Hz}$  gives a whistler wavelength of  $\approx 500$  to  $800 \text{ m}$ , the high-resolution attenuation profile is consistent with a boundary scale length of one or two whistler wavelengths. Short wavelengths also develop as  $B$  falls so that  $f_c$  approaches  $100 \text{ Hz}$ . These unexpected results suggest that whistler mode turbulence generated in the shocked solar wind can be strongly absorbed in the ionosphere of Venus. The maximum energy flux available from the wave damping process is given by the product of the wave energy density and the wave speed. In the case of orbit 4 (outbound) the 100-Hz averages yield a mean whistler mode flux of  $0.05 \text{ erg/cm}^2\text{-sec}$  that could provide a local energy source for ionospheric and atmospheric processes. However, the waves appear to have very large peak amplitudes, with corresponding sporadic enhancements in energy flux up to  $5 \text{ erg/cm}^2\text{-sec}$  (6).

F. L. SCARF

W. W. L. TAYLOR, I. M. GREEN  
Space Sciences Department, TRW  
Defense and Space Systems Group,  
Redondo Beach, California 90278

## References and Notes

1. These plasma oscillations are narrow-band electrostatic waves with frequency  $f = f_p = 9000 \sqrt{N} \text{ Hz}$ , where  $f_p$  is the electron plasma frequency and  $N$  is the electron density (electrons per cubic centimeter). For Earth, the connection between electron plasma oscillations and suprathermal electrons from the bow shock was first established by F. L. Scarf, R. W. Fredericks, L. A. Frank, and M. Neugebauer [*J. Geophys. Res.* **76**, 5162 (1971)].
2. M. K. Wallis, *Cosmic Electrodyn.* **3**, 45 (1972); *Planet. Space Sci.* **21**, 1647 (1973); R. E. Hartle, S. J. Bauer, C. S. Wu, *JAGA (Int. Assoc. Geomagn. Aeron.) Bull.* **34**, 569 (1973); S. J. Bauer et al., *Space Sci. Rev.* **20**, 413 (1977).
3. L. Bruce, personal communication.
4. The only instrumental effects that we have discovered to date involve the regular amplitude ripples that are evident in the high-resolution data of Fig. 2 after 1522. This effect is a measure of the sun-oriented anisotropy of the plasma sheath surrounding the spacecraft, which is not an equipotential. The observed ripple arises because the antenna on the spinning spacecraft is at a different angular position with respect to the sun during each successive sampling.
5. R. M. Thorne, *J. Geophys. Res.* **73**, 4895 (1968); H. B. Liemohn and F. L. Scarf, *ibid.* **69**, 883 (1964); C. Kennel, *Phys. Fluids* **9**, 2190 (1966).
6. This is quite large compared to the energy deposition in Earth's upper atmosphere. For instance, L. A. Frank and K. L. Ackerson [*J. Geophys. Res.* **76**, 3612 (1971)] showed that the energy input to the topside of Earth's auroral region is  $< 1 \text{ erg/cm}^2\text{-sec}$  during quiescent periods.
7. We thank P. Virobik, J. Atkinson, and E. Vrem for their invaluable assistance with the design, fabrication, and integration of the orbiter electric field detector; C. Hall and the staff of the Pioneer Venus Project at NASA Ames Research Center and Hughes Aircraft Company for their excellent support; C. Russell and his colleagues for assisting with the data processing; and C. Russell and L. Brace for allowing us to show their preliminary results here. We also acknowledge very helpful suggestions by F. V. Coroniti. This work was carried out under NASA contract NAS2-8809 and NAS2-9842.

16 January 1979

## Initial Observations of the Pioneer Venus Orbiter Solar Wind Plasma Experiment

**Abstract.** *Initial results of observations of the solar wind interaction with Venus indicate that Venus has a well-defined, strong, standing bow shock wave. Downstream from the shock, an ionosheath is observed in which the compressed and heated postshock plasma evidently interacts directly with the Venus ionosphere. Plasma ion velocity deflections observed within the ionosheath are consistent with flow around the blunt shape of the ionopause. The ionopause boundary is observed and defined by this experiment as the location where the ionosheath ion flow is first excluded. The positions of the bow shock and ionopause are variable and appear to respond to changes in the external solar wind pressure. Near the terminator the bow shock was observed at altitudes of  $\sim 4600$  to  $\sim 12,000$  kilometers. The ionopause altitude ranged from as low as  $\sim 450$  to  $\sim 1950$  kilometers. Within the Venus ionosphere low-energy ions (energy per unit charge  $< 30$  volts) were detected and have been tentatively identified as nonflowing ionospheric ions incident from a direction along the spacecraft velocity vector.*

The Ames Research Center Pioneer Venus orbiter plasma analyzer instrument is a quadrispherical, curved plate, electrostatic analyzer with five current collectors and electrometer amplifiers. It measures the ambient flux of plasma ions and electrons as a function of energy per unit charge ( $E/Q$ ) and direction of incidence. Ions are analyzed over two  $E/Q$  ranges: low energy from 0 to 250 V and high energy from 50 to 8000 V. Electrons are measured over the energy range 0 to 250 eV. A more complete description of this experiment is given in (1).

The results presented here were obtained during the first few weeks of orbital operation of the Pioneer Venus orbiter mission. During this period only real-time and incomplete data have been available, so the results are considered to be very preliminary.

Values of the peak speed of solar wind protons (Fig. 1) were obtained daily at approximately noon universal time (UT); they represent an interplanetary value taken several hours upstream from the

bow shock (2) on the inbound leg of each orbital pass. After Venus orbit insertion, the solar wind underwent a general decrease in speed until orbit 9. The large increase in solar wind at orbit 9 has been tentatively identified with the arrival at Venus of an interplanetary shock wave associated with a class 2B solar flare observed at 1909 UT on 11 December 1978. After the passage of this shock wave the solar wind convective pressure increased by approximately an order of magnitude; this was presumably responsible for the lowest ionopause altitude observed by this experiment in any orbit for which we have data. The prominent feature with a peak speed of  $\sim 760 \text{ km/sec}$  on orbit 17 is a high-speed solar wind stream and was probably not associated with any specific flare activity.

Figure 2 shows a comparison of an interplanetary solar wind ion spectrum and an ionosheath (3) spectrum obtained during relatively quiet conditions. These data were taken on day 344 (10 December) along the outbound trajectory of orbit 6. The interplanetary spectrum, ob-

tained at 1605:39 UT (spacecraft time), shows the  $H^+$  peak at  $\sim 400$  V and the  $He^{2+}$  peak at  $\sim 800$  V. A Maxwellian fit to the data gives a bulk speed  $v$  of 287 km/sec, a proton number density  $N$  of  $33 \text{ cm}^{-3}$ , and an isotropic proton temperature  $T$  of 20,700 K. For this case the components of the solar wind flow direction were  $+4.2^\circ$  in azimuthal angle (from the west when facing the solar direction) and  $+0.5^\circ$  in polar angle (from the north) measured perpendicular to the Venus orbital plane. The corresponding parameters for the ionosheath spectrum, obtained at 1536:46 UT, are  $v = 254$  km/sec,  $N = 87 \text{ cm}^{-3}$ ,  $T = 67,000$  K, azimuthal angle =  $6.5^\circ$ , and polar angle =  $+17.4^\circ$ .

A comparison of the free stream solar wind parameters with the postshock conditions shows a decrease in speed and a large increase in density and temperature, indicating the presence of a strong, detached, standing bow shock wave. The observed change in flow direction across the shock is wholly consistent with postshock flow around the blunt body of the Venus ionosphere.

Quiet conditions are not necessarily typical, but they serve to minimize temporal effects that can confuse the gross spatial features. That this pass took place under quiet conditions is indicated by the fact that the free stream solar wind parameters obtained on the inbound leg of this orbit were almost identical to those on the outbound leg. During more disturbed times (higher solar wind speeds) interplanetary conditions upstream of the bow shock frequently show complex spectra indicative of upstream disturbances, and the ionosheath temperatures frequently approach  $10^6$  K.

Figure 3 shows a sequence of  $E/Q$  spectra around periapsis on orbit 3. The first four spectra were obtained in the free stream solar wind upstream of the bow shock. The next two were obtained downstream of the bow shock in the Venus ionosheath. Both the lower levels of the peak currents associated with these spectra and the increased widths indicate thermalization of solar wind ions across the bow shock and conversion of streaming energy into particle heating. The two spectra with depressed current levels (at 1435 and 1443 UT) indicate the absence of measurable plasma ion flux in this energy range in the ionosphere below the ionopause. The subsequent spectra were obtained during the outbound portion of the orbit; they indicate the recrossing of the ionopause and finally, after 1536 UT, the reemergence of the spacecraft into the free stream solar wind.

Figure 4 shows the bow shock and ion-

opause locations observed for the first 29 orbits, based on preliminary information about the spacecraft trajectory and rotated into a common plane. Some possible bow shocks are indicated with extended limits or are omitted, and many

ionopause crossings are missing because of gaps in real-time data. These will be refined at a later date. In some of these instances, there were apparently repetitive shock crossings. Each indicated location or arc represents at least one bow

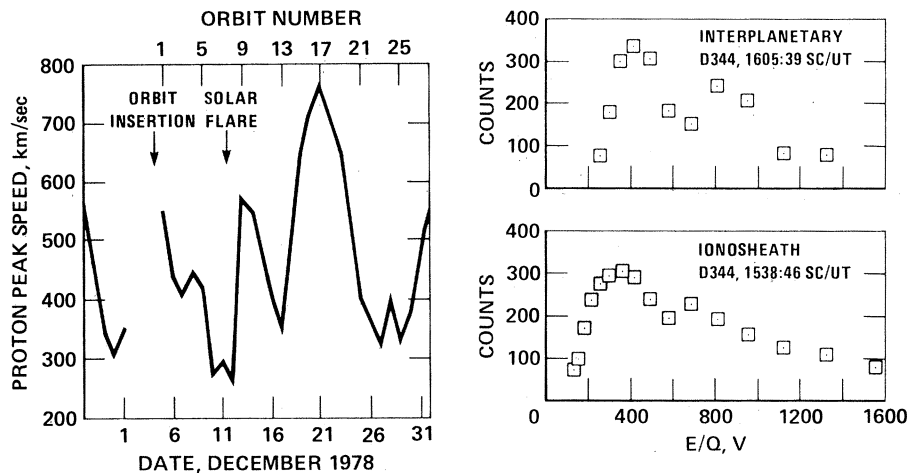


Fig. 1 (left). Daily solar wind proton peak speeds measured during December 1978. In most cases, the data were obtained near noon universal time for each orbit, upstream from the bow shock. Fig. 2 (right). Comparison of ionosheath and interplanetary ion spectra across the bow shock during the outbound leg of orbit 6. The parameters derived from these spectra by a Maxwellian fit are, for the interplanetary case,  $v = 287$  km/sec,  $N = 33 \text{ cm}^{-3}$ , and  $T = 20,700$  K; and for the ionosheath case,  $v = 254$  km/sec,  $N = 87 \text{ cm}^{-3}$ , and  $T = 67,000$  K.

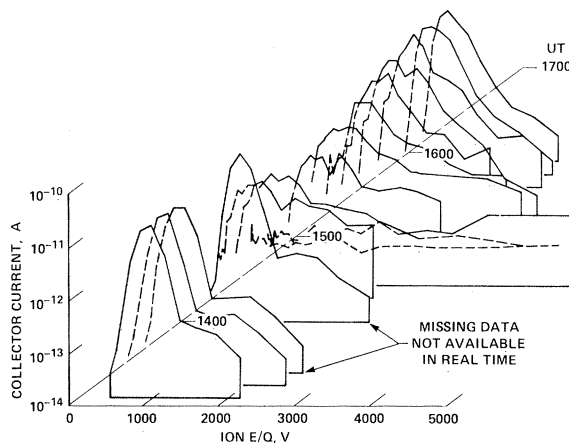


Fig. 3. Successive ion spectra for a portion of orbit 3 centered around periapsis, showing the change in spectral characteristics as the spacecraft passes from the interplanetary medium across the Venus bow shock, through the ionosheath, across the ionopause, and back across these same plasma regimes on the outbound leg.

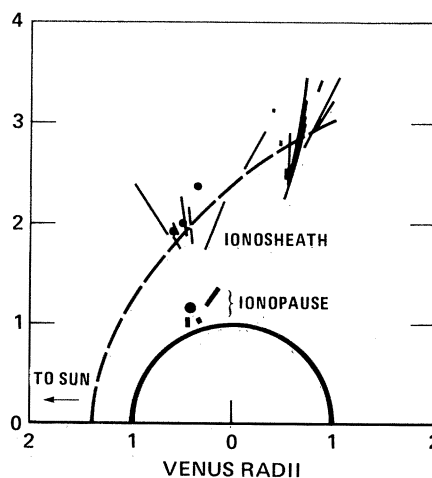


Fig. 4 (left). Bow shock and ionopause locations (or limits) plotted on a common plane, derived from available data from the plasma analyzer for the first 29 orbits. The dashed line indicates a calculated bow shock. Fig. 5 (right). Typical low-energy ion spectrum obtained in the ionosphere near periapsis on orbit 7. This spectrum is interpreted as representing nonflowing ionospheric ions incident from the ram direction and is consistent with ion species expected (7) in the Venus ionosphere.

shock crossing. The bow shock shape in Fig. 4 is the shape calculated by Spreiter *et al.* (4) for  $H/r_0 = 0.25$ , where  $H$  is the local atmospheric scale height and  $r_0$  is the distance from the ionopause nose to the center of Venus. Also, an upstream sonic Mach number of 8 and a ratio of specific heats of 5/3 were assumed. A shape associated with  $H/r_0 \sim 0.3$  would seem to be most representative of the measured bow shock locations, although they undoubtedly have been observed over a wide range of upstream sonic and Alfvén Mach numbers and solar wind pressures. The associated ionopause locations would imply a much thicker ionosphere (4) than the one observed, but inclusion of magnetohydrodynamic effects can result in lower-altitude ionopause surfaces (5). Another feature not included in the calculations would be effects of a possible thick ionopause boundary layer (3, 4, 6).

Observations in the ionosphere near periapsis were obtained by the plasma analyzer in its low-energy ion mode. Figure 5 shows the low-energy ion spectrum obtained between 0 and 40 V at  $\sim 1500$  UT on 11 December during orbit 7 when the spacecraft was at an altitude of  $\sim 310$  km. The first peak in the spectrum occurs at  $\sim 8$  V and the maximum of the broader second peak occurs at  $\sim 15$  V. Because of the measured angle of incidence, we interpret these data as indicating nonflowing ions apparently impinging from a direction along the ram velocity vector of the spacecraft. The ram speed at this time was  $\sim 9.7$  km/sec so that the peak in the spectrum at  $\sim 8$  V is consistent with an ion of mass 16, such as  $O^+$ , as indicated by the arrow in Fig. 5. Several ions could give rise to the second peak, and the mass positions of  $CO^+$ ,  $O_2^+$ , and  $CO_2^+$  ions expected at this altitude in the Venus ionosphere (7) are shown in Fig. 5.

The electron data obtained thus far are incomplete. However, preliminary results indicate the presence in the ionosheath of high-temperature electrons with typical energies in the range 50 to 100 eV. These observations seem consistent with heating of the solar wind electrons across the bow shock.

J. WOLFE

Space Science Division,  
NASA Ames Research Center,  
Moffett Field, California 94035

D. S. INTRILIGATOR

Physics Department, University of  
Southern California, Los Angeles 90007

J. MIHALOV, H. COLLARD

D. MCKIBBIN, R. WHITTEN, A. BARNES  
Space Science Division,  
NASA Ames Research Center

## References and Notes

1. L. Colin and D. M. Hunten, *Space Sci. Rev.* **20**, 500 (1977).
2. E. J. Smith, L. Davis, Jr., P. J. Coleman, Jr., C. P. Sonett, *J. Geophys. Res.* **70**, 1571 (1965); O. L. Vaisberg, A. Romanov, V. N. Smirnov, I. P. Karpinsky, B. I. Khazanov, B. V. Polenov, A. V. Bogdanov, N. M. Antonov, in *Physics of Solar Planetary Environments*, D. J. Williams, Ed. (American Geophysical Union, Washington, D.C., 1976), p. 904; S. J. Bauer, L. H. Brace, D. M. Hunten, D. S. Intriligator, W. C. Knudsen, A. F. Nagy, C. T. Russell, J. H. Wolfe, *Space Sci. Rev.* **20**, 413 (1977).
3. H. Pérez de Tejada and M. Dryer, *J. Geophys. Res.* **81**, 2023 (1976).
4. J. Spreiter, A. Summers, A. Rizzi, *Planet. Space Sci.* **18**, 1281 (1970).

5. J. Spreiter, in *NASA Spec. Publ. SP-397* (1976), p. 135.
6. C. T. Russell, *Geophys. Res. Lett.* **3**, 589 (1976).
7. H. A. Taylor *et al.*, *Science* **203**, 752 (1979).
8. We acknowledge the entire staff of the Pioneer Project Office for an excellent job, and particularly the following for their special attention to this experiment during various phases of the mission: J. Lepetich (orbiter plasma analyzer project manager), J. Cowley, J. Dyer, R. Fimmel, R. Jackson, B. Pittman, J. Pogue, D. Porter, and D. Sinnott. We also acknowledge Ball Brothers/WAL for building the instrument, particularly F. Hesse and G. Steele. Finally, we would like to thank the NOAA Space Environment Services for the real-time information concerning the solar flare on 11 December 1978.

16 January 1979

## Ionosphere of Venus: First Observations of the Dayside Ion Composition Near Dawn and Dusk

**Abstract.** *The first in situ measurements of the composition of the ionosphere of Venus are provided by independent Bennett radio-frequency ion mass spectrometers on the Pioneer Venus bus and orbiter spacecraft, exploring the dawn and duskside regions, respectively. An extensive composition of ion species, rich in oxygen, nitrogen, and carbon chemistry is identified. The dominant topside ion is  $O^+$ , with  $C^+$ ,  $N^+$ ,  $H^+$ , and  $He^+$  as prominent secondary ions. In the lower ionosphere, the ionization peak or  $F_1$  layer near 150 kilometers reaches a concentration of about  $5 \times 10^5$  ions per cubic centimeter, and is composed of the dominant molecular ion,  $O_2^+$ , with  $NO^+$ ,  $CO^+$ , and  $CO_2^+$ , constituting less than 10 percent of the total. Below the  $O^+$  peak near 200 kilometers, the ions exhibit scale heights consistent with a neutral gas temperature of about 180 K near the terminator. In the upper ionosphere, scale heights of all species reflect the effects of plasma transport, which lifts the composition upward to the often abrupt ionopause, or thermal ion boundary, which is observed to vary in height between 250 to 1800 kilometers, in response to solar wind dynamics.*

Bennett radio-frequency (rf) ion mass spectrometers carried by the Pioneer Venus bus and orbiter spacecraft are providing the first detailed in situ measurements of the dayside ion composition. The orbiter instrument began returning daily profiles of the planetary ionosphere starting on 5 December 1978, with an initial periapsis of 379 km at  $17.0^\circ N$  latitude, solar zenith angle ( $\chi$ ) of  $63^\circ$ , and an orbital inclination of  $105^\circ$ . The orbit geometry is such that inbound passes approach periapsis from the north, with an orbit plane precession of about  $1.5^\circ$  per day toward the dusk terminator. On 9 December, the bus instrument obtained a single profile of the dawnside ionosphere, providing measurements down to about 128 km ( $\chi = 59^\circ$ ;  $42^\circ S$  latitude), below which instrument performance degraded rapidly because of the impact with the dense neutral atmosphere.

The identical bus and orbiter instruments (BIMS and OIMS, respectively) (1) are designed to provide detailed measurements of the concentration and variability of as many as 16 possible ion species, selected originally as the most probable constituents from theoretical considerations. As the instrument explores for, and detects the presence of, a

given species, an in-flight analysis is made of each ion measurement to account for the effects of spacecraft velocity, skin charge, and bulk ion drift. This analysis also permits the recovery of suprathermal ion characteristics induced by the interaction of the solar wind and the ionosphere. The instrument operating modes are automatically sequenced to alternately explore, then adapt to, repeated measurements of prominent ions. The temporal and spatial sampling resolution for a given ion thus varies, according to the number and relative abundance of species detected. In general, prominent ions are measured at a rate of about once per second, corresponding to a height resolution of a few kilometers between successive samples.

An example of the resolution provided in the ion measurements is given in Fig. 1, in which all samples of each of three prominent ions ( $O^+$ ,  $O_2^+$ , and  $H^+$ ) are plotted. To facilitate the data processing, smooth profiles have been constructed as a best fit to the measurements, and such profiles are used in the further illustrations in this and in (2). The spread in the raw data points reflects instrument sampling adjustments as well as natural variations, and thus subsequent detailed